Published in final edited form as:
Dev Biol. 2009 August 15; 332(2): 309–324. doi:10.1016/j.ydbio.2009.05.575.

Four Distinct Phases of Basket/Stellate Cell Migration after Entering their Final Destination (the Molecular Layer) in the Developing Cerebellum

D. Bryant Cameron[1], **Kazue Kasai**[2], **Yulan Jiang**[1], **Taofang Hu**[1], **Yoshinaga Saeki**[2], and **Hitoshi Komuro**[1]

[1]Department of Neurosciences, Lerner Research Institute, Cleveland, Ohio 44195, USA

[2]Dardinger Laboratory for Neuro-oncology and Neurosciences, Department of Neurological Surgery and Comprehensive Cancer Center, The Ohio State University, Columbus, Ohio, 43210, USA

Abstract

In the adult cerebellum, basket/stellate cells are scattered throughout the ML, but little is known about the process underlying the cell dispersion. To determine the allocation of stellate/basket cells within the ML, we examined their migration in the early postnatal mouse cerebellum. We found that after entering the ML, basket/stellate cells sequentially exhibit four distinct phases of migration. First, the cells migrated radially from the bottom to the top while exhibiting saltatory movement with a single leading process (Phase I). Second, the cells turned at the top and migrated tangentially in a rostro-caudal direction, with an occasional reversal of the direction of migration (Phase II). Third, the cells turned and migrated radially within the ML at a significantly reduced speed while repeatedly extending and withdrawing the leading processes (Phase III). Fourth, the cells turned at the middle and migrated tangentially at their slowest speed, while extending several dendrite-like processes after having completely withdrawn the leading process (Phase IV). Finally, the cells stopped and completed their migration. These results suggest that the dispersion of basket/stellate cells in the ML is controlled by the orchestrated activity of external guidance cues, cell-cell contact and intrinsic programs in a position-and time-dependent manner.

Keywords

stellate cell; basket cell; inhibitory interneurons; neuronal cell migration; cerebellum; early postnatal mice; time-lapse imaging; brain slices

Introduction

In the developing brain, the majority of immature neurons migrate from their birthplace to their final destination (Rakic, 1990; Rakic et al., 1994; Nadarajah and Parnavelas, 2002; Komuro and Yacubova, 2003; Ghashghaei et al., 2006). This active movement of immature neurons is

To whom correspondence should be addressed. Dr. Hitoshi Komuro, Department of Neurosciences/NC30, Lerner Research Institute, The Cleveland Clinic Foundation, 9500 Euclid Avenue, Cleveland, OH 44195, USA, Tel: (216) 444-4497, Fax: (216) 444-7927, E-mail: E-mail: komuroh@ccf.org.

essential for the formation of neuronal cytoarchitecture and proper differentiation (Rakic, 2000; Guerrini and Filippi, 2005; Kerjan and Gleeson, 2007; Pang et al., 2008). Excitatory neurons and inhibitory neurons originate from different regions of the brain, and exhibit different modes of migration (Nadarajah and Parnavelas, 2002; Marin and Rubenstein, 2003; Tashiro et al., 2007; Tanaka et al., 2009). For example, in the developing cerebrum, excitatory neurons, which are born in the ventricular and subventricular zone, migrate radially to the cortical plate, while inhibitory neurons, which are born in the medial and lateral ganglionic eminence, migrate tangentially to the cortical plate (Marin and Rubenstein, 2001; Anderson et al., 2001; Ang et al., 2003; Kriegstein and Noctor, 2004). In the developing cerebellum, the migration of excitatory interneurons (such as granule cells) and inhibitory projection neurons (such as Purkinje cells) has been extensively examined (Rakic, 1971; Rakic and Komuro, 1995; Komuro and Rakic, 1998b; ten Donlelaar et al., 2003; Yacubova and Komuro, 2003; Botia et al., 2007; Kumada et al., 2007; Jiang et al., 2008; Cameron et al., 2009), but little is known about the migration of inhibitory interneurons (such as basket cells and stellate cells).

Both basket cells and stellate cells are GABAergic interneurons and located in the molecular layer (ML) of the cerebellum. They receive an excitatory synaptic input from granule cell axons (parallel fibers) and their axons make an inhibitory synapse with Purkinje cells. Both basket cells and stellate cells are scattered throughout the ML, but there is a bias in their allocation: the majority of basket cells are located in the bottom half of the ML, while the majority of stellate cells are located in the top half (Rakic, 1973). Until recently, the origin of basket cells and stellate cells has been controversial. The prevailing view has been that they share a common ancestry with cerebellar granule cells and originate from the external granular layer (EGL) (Miale and Sidman, 1961; Altman, 1972a,b). However, recent studies have clarified this long-standing conundrum of cerebellar histogenesis (Otero et al., 1993; Napieralski and Eisenman, 1993; Hallonet and Le Douarin, 1993; Zhang and Goldman, 1996a,b; Maricich and Herrup, 1999; Milosevic and Goldman, 2002, 2004; Yamanaka et al., 2004; Leto et al., 2006). The progenitors of both cells originate from the neuroepithelium of the fourth ventricle. They first migrate outward to reach the deep white matter (WM) of the embryonic cerebellum, and then continue to divide in the deep WM as well as in the folial WM during their migration.

It has been demonstrated that basket cells and stellate cells migrate from the deep WM through the folial WM, the internal granular layer (IGL) and the Purkinje cell layer (PCL) to the ML (their final destination) during early postnatal development (Zhang and Goldman, 1996a,b; Milosevic and Goldman, 2004), but little is known about how the cells complete their migration in the ML. In this study, with the use of real-time observation of cell movement and a herpes simplex virus (HSV) amplicon vector HGY, which expresses EGFP under the control of the HSV immediate-early (IE) 4/5 promoter, we examined the migration of basket cells and stellate cells in the ML of the early postnatal mouse cerebellum. We found that in the ML, basket cells and stellate cells sequentially go through four distinct phases of migration before completing their migration.

Materials and Methods

All procedures were in strict accordance with the NIH Guide for the Care and Use of Laboratory Animals and were approved by the Institutional Animal Care and Use Committee of the Cleveland Clinic Foundation and the Ohio State University

Plasmid construction

A HSV amplicon plasmid pHGY was constructed from pHGCX (Saeki et al., 2003; Kasai and Saeki, 2006) by removing the cytomegalovirus IE promoter and inserting a pair of *FRT* and *loxP* sites. pHGY is a pBR322-based amplicon plasmid and expresses enhanced green

fluorescent protein (EGFP, BD biosciences, San Jose, CA) under the control of the HSV IE4/5 promoter.

Cell culture and vector production

Vero 2-2 packaging cells (Smith et al., 1992) were kindly provided by Rozanne M. Sandri-Goldin (University of California, Irvine, CA) and cultured in Dulbecco's modified Eagle's medium (DMEM) supplemented with 10% fetal bovine serum (FBS), penicillin (100 U/ml), and streptomycin (100 (μg/ml). G16-9 titration cells (Kasai and Saeki, 2006) were maintained in DMEM supplemented with 10% FBS, penicillin (100 U/ml), streptomycin (100 (μg/ml), and hygromycin B (200 (μg/ml). All cells were cultured at 37 °C in a CO_2 incubator (95 % Air and 5% CO_2). HSV amplicons were packaged using the improved helper virus-free packaging system as described previously (Saeki et al., 2001, 2003; Kasai and Saeki, 2006). Briefly, 2-2 cells (plated at approximately 90% confluence in 6-cm culture dishes) were transfected with 0.6 (μg pHGY DNA, 0.2 μg pEBH-ICP27 DNA, and 2 μg fHSVΔpacΔ27−0 + DNA using LipofectAMINE Plus (Invitrogen, Carlsbad, CA) according to the manufacturer's protocol. Three days later, the transfected cells and medium were harvested, and the crude HGY vector stocks were concentrated by ultracentrifugation at 75,000×*g* for 3 hours at 4°C over a 25% (wt/vol) sucrose cushion. The pellet was then resuspended in Hanks' balanced salt solution and stored at −80°C until use. The titer (green fluorescent protein transducing units [TU]/ml) of each vector stock was determined on G16-9 cells at 24 hours after infection

Monitoring cell migration in cerebellar slice preparations

Cerebella of postnatal day (P) 5–14 mice (CD-1, both sexes) were sectioned transversely or sagittally into 180 μm-thick slices on a vibrating blade microtome (VT1000S, Leica Instruments) (Komuro and Rakic, 1992, 1993, 1995; 1998a; Komuro et al., 2001). Cerebellar slices were placed on 24-mm diameter polyester membrane inserts (0.4 μm pore size, Corning Inc.) in 6 well plates (Corning Inc.). The bottom of each plate was filled with 2.5 ml of culture medium, which consisted of DMEM/F12 (Invitrogen) with N2 supplement, penicillin (90 U/ml) and streptomycin (90 μg/ml). Fifteen μl of the culture medium with 0.7 μl of 2×10^8 TU/ml of HGY amplicon vector was added to the center of the top surface of each slice. The slices were subsequently put in a CO_2 incubator (37°C, 95% air, 5% CO_2). Twenty-four hours after sectioning, slices were transferred and placed on 35 mm-glass bottom microwell dishes (MatTek Co.) with 2.0 ml of the culture medium. The dishes were placed into the chamber of a micro-incubator (PDMI-2, Harvard Apparatus) attached to the stage of a confocal microscope (Leica). The chamber temperature was kept at 37.0 ± 0.5°C, and the slices were provided with constant gas flow (95% air, 5% CO_2). To prevent movement of the slices during observation, a nylon net glued to a small silver wire ring was placed over the preparations.

A laser scanning confocal microscope (TCS SP, Leica) was used to visualize EGFP-expressing cells in the slices (Komuro and Rakic, 1998a; Komuro et al., 2001; Komuro and Kumada, 2005; Kumada et al., 2006; Cameron et al., 2007). The use of this microscope permitted high-resolution imaging of EGFP-expressing cells up to 100 μm deep within the tissue slices. The tissue was illuminated with 488-nm wavelength light from an argon laser through an epifluorescence inverted microscope equipped with a 40x oil-immersion objective, and fluorescence emission was detected at 530 ±15 nm. Image data were collected at an additional electronic zoom factor of 1.0–2.0. To determine the location of EGFP-expressing cells within the ML, the EGL-ML border and the ML-PCL border, at the beginning and the end of each recording session, fluorescence images and transmitted images were simultaneously recorded with 40x magnification. To avoid the injured cells located near the sectioning surfaces, we examined the migration of EGFP-expressing cells located 15–50 μm below the surface of each slice. To monitor migration and morphological changes, images of EGFP-expressing cells in

up to 40 different focal planes along the z-axis were collected with laser scans every 30 minutes for up to 70 hours.

The long-term observation of cell movement allowed us to examine the behavior of EGFP-expressing cells (stellate/basket cells) from the entrance into the ML to the completion of the migration within the ML. Therefore, in this study, the average speed of migration and the average transit time in the four different phases were obtained from the same EGFP-expressing cells (stellate/basket cells).

Monitoring cell migration in microexplant cultures

Cerebella of P0-P3 mice (CD-1, both sexes) were placed in ice-chilled Hanks' balanced salt solution, and freed from meninges and choroid plexus (Komuro and Rakic, 1996, 1999; Yacubova and Komuro, 2002a,b; Kumada et al., 2008, 2009). Cerebellar slices were made with a surgical blade. Rectangular pieces (50–100 μm) were dissected out from the slices under a dissecting microscope. Small pieces of cerebellum were placed on 35 mm-glass bottom microwell dishes (MatTek Co.), which had been coated with poly-L-lysine (100 μg/ml)/ laminin (20 μg/ml), with 50 μl of the culture medium. Dishes were put in a CO_2 incubator (37° C, 95% air, 5% CO_2). Two hours after plating, 1 ml of the culture medium with or without 2 μl of 2×10^8 TU/ml of HGY amplicon vector was added to each dish. The incubation medium consisted of DMEM/F12 (Invitrogen) with N2 supplement, penicillin (90 U/ml) and streptomycin (90 μg/ml). Ten hours after plating, the culture medium was replaced by 1 ml of the fresh culture medium without HGY amplicon vector. Twenty-four hours after plating, dishes were transferred into the chamber of a micro-incubator (PDMI-2, Harvard Apparatus) attached to the stage of a confocal microscope (TCS SP, Leica). The chamber temperature was kept at 37.0 ± 0.5°C using a temperature controller (TC-202, Harvard Apparatus) and the cells were provided with constant gas flow (95% air, 5% CO_2). The cells were illuminated with 488-nm wavelength light from an argon laser through an inverted microscope equipped with a 20x oil-immersion objective or a 40x oil-immersion objective. Fluorescence images for EGFP-expressing cells (at 530+15 nm) and transmitted images for EGFP-negative cells were simultaneously collected (Yacubova and Komuro, 2002a; Kumada and Komuro, 2004). Images of the cells in a single focal plane were collected with laser scans every 60 seconds for up to 2 hours. The distance traveled by the cells was defined as the absolute value of the change in its position during the entire time-lapse session.

Immunohistochemistry of GAD67

After an anesthetic overdose, P6, P10 and P14 mice (CD-1, both sexes) were perfused transcardially with phosphate buffer saline (PBS) (pH 7.4), followed by 4 % paraformaldehyde in PBS. Cerebella were dissected and post-fixed overnight at 4°C with the same fixative solution. Then, cerebella were stored for 12 hours at 4°C in a solution of PBS containing 15 % and 30 % sucrose successively. Thereafter, cerebella were cut at 30 μm in the sagittal plane with a cryostat (CM 3050 S, Leica). Sections were placed in 20% Triton X-100 in PBS and shaken for one hour at a room temperature. Subsequently, sections were blocked in 1.5% normal donkey serum and 0.2% Triton X-100 in PBS for 30 minutes, and incubated with mouse anti-GAD67 antibody (1:1500, CHEMICON International) for 1–2 hours. After rinsing three times with PBS, sections were incubated for 30 minutes at a room temperature with a fluorescein-conjugated-donkey anti-mouse IgG (1:200, Jackson ImmunoResearch Laboratories, Inc.) and TO-PRO-3 (1:1000, Invitrogen) for nuclear staining. Finally, sections were rinsed in PBS (3 times), and mounted in PBS/glycerol (1/1). Fluorescent signals for GAD67 and nuclear staining were detected and processed using a laser scanning confocal microscope (TCS SP, Leica).

To determine the cell type of EGFP-expressing cells in the ML, after completing real-time observation of cell migration, cerebellar slices were fixed with 4 % paraformaldehyde in PBS for 60 minutes at a room temperature. Then, slices were blocked in 1.5% normal donkey serum and 0.2% Triton X-100 in PBS for 30 minutes, and incubated with mouse anti-GAD67 antibody (1:1500, CHEMICON International) for 1–2 hours. After rinsing three times with PBS, slices were incubated with rhodamine red-X-conjugated-donkey anti-mouse IgG (1:200, Jackson ImmunoResearch Laboratories, Inc.) for 30 minutes at a room temperature. Thereafter, slices were rinsed in PBS (3 times), and mounted in PBS/glycerol (1/1). Fluorescent signals for GAD67 (rhodamine red-X) and EGFP were simultaneously detected and processed using a laser scanning confocal microscope

Statistical analysis

Statistical differences were determined using Student's *t*-test. Statistical significance was defined at $P < 0.05$ or $P < 0.01$.

Results

First, we determined the time period during which immature basket cells and stellate cells enter the ML of the developing cerebellum. To this end, because basket cells and stellate cells are the only GABAergic cells whose somata are located in the ML (Yip et al., 2008), we used an antibody for glutamic acid decarboxylase67 (GAD67), which is one of the isoforms of GAD that plays a role in synthesizing γ-aminobutyric acid (GABA) from glutamate. In this study, basket cells and stellate cells were counted collectively as basket/stellate cells because immature basket cells and stellate cells were not classified morphologically. Immunohistochemical staining for GAD67 revealed that as early as P6, a small number of basket/stellate cells is already present in the ML (Fig. 1A1–3 and B1–3). In the P10 and P14 cerebella, many basket/stellate cells were scattered throughout the ML (Fig. 1C1–3, D1–3, E1–3, and F1–3). The number of basket/stellate cells per 100 μm-length of the ML systematically increased from 1.2±0.8 cells at P6 to 11.0±1.6 cells at P10 to 33.1±2.7 cells at P14 (Supplementary Fig. 1). Since no cell division is observed in the ML of the developing cerebellum (Miale and Sidman, 1961; Fujita et al., 1966; Fujita, 1967), the results indicated that large numbers of basket/stellate cells enter the ML during the period of P6–P14.

Next, we examined whether the use of an HSV amplicon vector HGY, which expresses EGFP under the control of the HSV IE4/5 promoter (Saeki et al., 2003; Kasai and Saeki, 2006), affects the migration of immature cells. To this end, we used the microexplant cultures of P0-P3 mouse cerebella (Yacubova and Komuro, 2002a,b; Kumada et al., 2006, 2009). In the cultures, 22 hours after adding the HGY amplicon vector to the culture medium (24 hours after *in vitro*), 18 % of the cells (51/283 cells) expressed EGFP (Supplementary Fig. 2A1–A3). The real-time observation of cell movement revealed that there is no statistically significant difference in the average speed of migration between EGFP-expressing cells and EGFP-negative cells (Supplementary Fig. 2B), suggesting that the application of an HGY amplicon vector does not alter the migration of cerebellar cells.

After confirming the usefulness of an HGY amplicon vector for cell labeling, we first examined how basket/stellate cells enter the ML. To address this issue, we chose EGFP-expressing basket/stellate cells which were located at the PCL-IGL border. In this series of experiments, all EGFP-expressing cells whose migration had been examined were stained with an antibody for GAD67 after the completion of time-lapse imaging to determine the cell type (Supplementary Fig. 3). We only included the data obtained from GAD67 positive-EGFP-expressing cells (basket/stellate cells) in this study. A typical example of basket/stellate cell migration from the IGL through the PCL to the top of the ML is provided in Fig.2. During the period of 25.0–26.5 hours after *in vitro*, a basket/stellate cell, which had a vertically elongated

soma with a thick leading process, moved radially from the top of the IGL through the PCL to the bottom of the ML (Fig. 2A1). During the period of 26.5–27.5 hours after *in vitro*, the cell continuously migrated radially towards the top of the ML (Fig. 2A1, B1). At 28 hours after *in vitro*, the tip of the leading process turned horizontally towards the right side of the photo (Fig. 2A1, B1). During the period of 28–28.5 hours after *in vitro*, the leading process extended horizontally, while the soma migrated radially towards the top of the ML until reaching the point where the leading process turned horizontally (Fig. 2A1, B2). During the period of 28.5–29.5 hours after *in vitro*, the soma changed orientation from radial to horizontal, and then migrated tangentially near the EGL-ML border (Fig. 2A1, B2, B3). Because this slice was obtained from sagittal sections of the cerebellum, the cell migrated perpendicular to the folia (perpendicular to the direction of the extension of parallel fibers). At 32 hours after *in vitro*, the branch of the leading process crossed the EGL-ML border, which was determined by a simultaneous recording of fluorescent images and transmitted images (as shown in Fig. 2A2–A4), while the cell body never entered the EGL. All basket/stellate cells, which were initially located at the top of the IGL and had an vertically-elongated cell body with a leading process, reached the top of the ML within 10 hours after the initiation of the observation (n=36). Among them, 81% of the cells (29 out of 36 cells) migrated radially towards the top of the ML, while 19 % of the cells (7 out of 36 cells) migrated obliquely towards the top. During the migration towards the top of the ML, stellate/basket cells exhibited the saltatory movement (Fig.2 C1, C2). The average speed was ~14.9±1.1 μm/hr (n=36) (Supplementary Fig. 4), and the average transit time to move from the PCL-ML border to the top of the ML was ~7.4±1.5 hours (n=36). Taken together, these results indicated that basket/stellate cells migrate radially or obliquely from the top of the IGL through the PCL to the top of the ML. After reaching the top of the ML, the cells turned and then migrated tangentially in the rostro-caudal direction (perpendicular to the folia). The results also suggest the existence of attractive cues for basket/stellate cell migration in the top of the ML and repulsive cues in the EGL.

How do basket/stellate cells migrate tangentially at the top of the ML? To answer the question, we followed basket/stellate cell migration at the top of the ML. Two typical examples of basket/stellate cell migration at the top of the ML are provided in Fig. 3 and Fig. 4. The first example represents the long-lasting tangential migration of basket/stellate cells at the top of the ML while altering the speed of movement (Fig. 3). During the period of 31.0–39.5 hours after *in vitro*, a basket/stellate cell, which had a horizontally oriented cell body and a horizontally extending leading process, migrated tangentially in the rostro-caudal direction (perpendicular to folia) at the top of the ML (Fig. 3A, B1, B2). The speed of cell movement dynamically fluctuated with a range between 1.2 μm per 0.5 hour (during the period of 32.5–33.0 hours after *in vitro*) and 20.5 μm per 0.5 hour (during the period of 38.0–38.5 hours after *in vitro*) (Fig. 3C1, C2). The second example represents the reversal of the tangential migration of basket/stellate cells at the top of the ML (Fig. 4). During the period of 32.0–37.5 hours after *in vitro*, the horizontally oriented soma of a basket/stellate cell migrated tangentially towards the rostral direction (the right side of the photo) at the top of the ML (Fig. 4A, B1). At 38.0 hours after *in vitro*, the soma reversed the direction of movement and then started to migrate towards the caudal direction (the left side of the photo) during the period of 38.0–40.5 hours after *in vitro* (Fig. 4A, B2, C1, C2). At 41.0 hours after *in vitro*, the soma again reversed the direction of movement and migrated towards the rostral direction during the period of 41.0–43.5 after *in vitro* (Fig. 4A, B3, C1, C2). At the top of the ML of the P6-P14 cerebella, all basket/stellate cells we examined migrated tangentially in the rostro-caudal direction but not in the medio-lateral direction. Furthermore, ~13 % of basket/stellate cells (5 out of 39 cells) exhibited reversal of the direction of migration during tangential migration at the top of the ML. The average speed of the tangential migration at the top of the ML was ~15.4±1.3 μm/hr (n=39) (Supplementary Fig. 4).

After a prolonged tangential migration (~16.8±1.9 hours; n=39) at the top of the ML, basket/stellate cells changed their direction of migration from tangential to radial (Fig. 5). Two typical examples of the radial migration of basket/stellate cells within the ML after a prolonged tangential migration are provided in Fig. 5 and Fig. 6. The first example represents the transition from tangential migration to radial migration at the top of the ML (Fig. 5). During the period of 45.0–48.5 hours after *in vitro*, while a basket/stellate cell soma moved tangentially at the top of the ML, the tip of the leading process turned and then extended towards the bottom of the ML (Fig. 5A, B1). At 49.0 hours after *in vitro*, the soma changed orientation from horizontal to radial, and then started to migrate radially towards the bottom of the ML during the period of 49.5–57.5 hours after *in vitro* (Fig. 5A, B1–4). During the radial migration, the tip of the leading process was bifurcated, and the two branches extended in opposite directions (Fig. 5A, B2–4). At 53.0 hours after *in vitro*, the right side of the branch started to collapse and then withdrew (Fig. 5A, B3). The soma repeatedly became stationary and moved at a significantly reduced rate (3.7 μm/hours) (Fig. 5C1, C2). The second example represents the reversal of radial migration of basket/stellate cells after reaching the bottom of the ML (Fig. 6). During the period of 53.0–59.0 hours after *in vitro*, at the bottom of the ML, the horizontally-oriented soma of a basket/stellate cell, which had migrated radially from the top of the ML to the bottom for more than 12 hours, slowly moved tangentially towards the direction of the extension of a horizontal process (the rostral direction) (Fig. 6A, B1). At 59.5 hours after *in vitro*, the soma changed the direction of migration from tangential to radial, and then migrated radially towards the top of the ML during the period of 60–65.5 hours after *in vitro* (Fig. 6A, B2–4). The leading processes repeatedly extended and withdrew multiple branches (Fig. 6A, B1–4), while the soma exhibited a stop-and-go type movement (Fig. 6C1, C2). The average speed of radial migration from the top of the ML to the bottom and from the bottom to the top after the reversal of the direction of movement were ~7.2±1.1 μm/hr (n=34) (Supplementary Fig. 4). Collectively, these results indicated that after changing the direction of migration from tangential to radial at the top of the ML, basket/stellate cells again exhibit radial migration within the ML at a reduced rate, while they repeatedly extend and withdraw the multiple branches of the leading process.

In the adult cerebellum the cell body of basket/stellate cell orients horizontally throughout the ML. How do radially-oriented somata of basket/stellate cells become horizontally-oriented in the ML? Two typical examples of basket/stellate cells showing the final stage of migration in the ML are provided in Fig. 7. During the period of 66–67 hours after *in vitro*, the vertically oriented soma of a basket/stellate cell, which had migrated radially within the ML for more than 16 hours, turned towards the caudal direction (the left side of the photo), and then migrated tangentially at the middle of the ML during the period of 67–68 hours after *in vitro* (Fig. 7A, B, C1, C2). In the other example, the vertically oriented soma of a basket/stellate cell, which had migrated radially in the ML for 17 hours, turned towards the rostral direction (the right side of the photo), and then migrated tangentially at the middle of the ML (Fig. 7D, E1, E2, F1, F2). The average transit time from the initiation of radial migration at the top of the ML to the initiation of tangential migration at the middle was ~19.3±2.3 hours (n=34). These results indicated that after a prolonged radial migration within the ML, basket/stellate cells change the orientation of their soma from radial to horizontal at the middle of the ML.

What is the initial sign of the termination of basket/stellate cell migration in the ML? Typical examples showing morphological changes of basket/stellate cells during the final phase of their migration within the ML are provided in Fig. 8 and Fig. 9. During the period of 71.0–75.0 hours after *in vitro*, a basket/stellate cell, which had migrated tangentially towards the caudal direction (the left side of the photo) at the middle of the ML for 4 hours, gradually withdrew the leading process (Fig. 8A, B1, B2, C1, C2). After completely withdrawing the leading process, the cell emitted short processes from the soma, while the soma migrated tangentially during the period of 75.0–76.5 hours after *in vitro* (Fig. 8A, B3). Interestingly, the short

processes emitted from the soma continuously extended and became dendrite-like processes, while the soma migrated tangentially at their slowest speed (Fig. 9). For example, during the period of 75.0–78.5 hours after *in vitro*, the horizontally oriented somata of basket/stellate cells (a and b in Fig. 9A), which had migrated tangentially for more than 6 hours in the middle of the ML, continuously extended their processes, while both somata exhibited small forward and backward movement (Fig. 9A, B1, B2, C1, C2, D1, D2, E1, E2). At 78.5 hours after *in vitro*, the processes of both cells became dendrite-like processes (Fig. 9A, B2, C2). Taken together, these results indicate that the retraction of the leading process and subsequent extension of dendrite-like processes from the soma are the initial signs of the completion of basket/stellate cell migration. Furthermore, these results also suggest that the extension of dendrite-like processes towards multiple directions plays a role in searching for the external stop signals for cell movement.

How do basket/stellate cells complete their migration? A typical example of the termination of basket/stellate cell migration is provided in Fig. 10. During the period of 80.0–81 hours after *in vitro*, the horizontally oriented soma of a basket/stellate cell, which had migrated tangentially at the middle of the ML for more than 9 hours, slowly moved towards the caudal direction (the left side of the photo) (Fig. 10A, B1). At 81 hours after *in vitro*, the soma stopped moving and became completely stationary (Fig. 10C1, C2), while the tip of the dendrite-like processes repeatedly extended and withdrew (Fig. 10A, B1, B2). When basket/stellate cells completed their migration at the middle of the ML, their somata were always oriented horizontally in the rostro-caudal direction. The average speed during the final stage of tangential migration at the middle of the ML was ~4.6+0.9 μm/hr (n=38) (Supplementary Fig. 4). The average transit time from the initiation of tangential migration at the middle of the ML to the completion of migration was ~10.2±1.2 hours (n=38). Collectively, the results indicate that basket/stellate cells complete their migration at the middle of the ML, while extending and withdrawing dendrite-like processes in multiple directions. Furthermore, the results suggest that stop signals for basket/stellate cell migration are present in the middle of the ML. Moreover, the results also suggest that the timing of the completion of basket/stellate cell migration overlaps with the timing of the initiation of their differentiation.

Discussion

Our present study demonstrates that in the ML of the early postnatal mouse cerebellum, immature basket/stellate cells sequentially go through four distinct phases of migration before completing their migration (as schematically shown in Fig. 11). First, after entering the ML through the PCL, basket/stellate cells migrate radially toward the top of the ML for ~7.4 hours with a vertically-elongated soma and a single leading process (Phase I). Upon reaching the top of the ML, the cells turn and change orientation from vertical to horizontal. Second, the cells migrate tangentially in the rostro-caudal direction (perpendicular to the direction of the extension of the parallel fibers and folia) at the top of the ML for ~16.8 hours with a horizontally-elongated soma and a single leading process (Phase II). At the end of Phase II, the cells turn and change orientation from horizontal to vertical. Third, the cells migrate radially within the ML from the top to the bottom and vice versa for ~19.3 hours at a reduced speed, while repeatedly extending and withdrawing the leading processes (Phase III). After prolonged radial migration within the ML, the cells turn and change orientation from vertical to horizontal in the middle of the ML. Fourth, the cells tangentially migrate in the rostro-caudal direction at their slowest speed for ~10.2 hours in the middle of the ML, while completely withdrawing the leading process and subsequently extending several dendrite-like processes in multiple directions (Phase IV). Finally, the cells stopped and completed their migration at the middle of the ML. Taken together, our present results reveal that in the ML, immature stellate/basket cells alter the mode, rate and direction of migration in a position-dependent and time-dependent manner before completing their migration.

After entering the ML, immature stellate/basket cells exhibit prolonged migration (~53.7 hours from Phase I to Phase IV). To date, little is known about why basket/stellate cells loiter in the ML for an extended period of time, but there are some hints. First, it has been reported that there is a high density of immature basket/stellate cells seen directly adjacent to the EGL of the developing cerebellum, which is clearly distinct from the even spacing of mature basket/stellate cells in the adult cerebellum (Weisheit et al., 2006). The high density of immature basket/stellate cells at the top of the ML suggests that basket/stellate cells migrate prematurely into the ML, where they sojourn next to the EGL, before they ultimately translocate to their final position (Weisheit et al., 2006). The prolonged migration of stellate/basket cells may provide a time for their differentiation, which may be required for proper distribution. Second, Rakic assumed that basket/stellate cells must remain in a postmitotic but undifferentiated state until the granule cell axons (parallel fibers) with which they will be ultimately connected become generated (Rakic, 1973). The prolonged migration of stellate/basket cells may provide a time for granule cells to form the parallel fibers. Third, once having passed the PCL, sequentially generated basket/stellate cells may be required to spend a certain time to successively occupy those areas of the ML not yet colonized by their siblings (Rakic, 1973). Fourth, the prolonged migration of stellate/basket cells may be controlled by intrinsic programs as described in the migration of cerebellar granule cells (Yacubova and Komuro, 2002a; Kumada et al., 2008, 2009). For example, intrinsic programs may control the timing of the expression of receptors which recognize external stop signals. Collectively, present and previous studies suggest that the prolonged migration of immature basket/stellate cells in the ML is a prerequisite for cell dispersion and maturation. Interestingly, it has been reported that in the embryonic mouse cerebrum, GABAergic interneurons linger in the marginal zone for a few days before approaching their final destination in the cortical plate (Tanaka et al., 2006, 2009). Therefore, GABAergic interneurons, such as basket/stellate cells, may be required to loiter on the way to their final destination in the developing brain.

The mechanisms underlying the control of stellate/basket cell migration in the ML are largely unknown, but there are possible candidates. First, in the microexplant cultures of the early postnatal cerebellum, basket/stellate cells exhibit repulsive behavior against Netrin1 (Guijarro et al., 2006). Interestingly, Netrin1 is highly present in the EGL of the early postnatal mouse cerebellum (Guijarro et al., 2006). Our present study revealed that at the top of the ML, basket/stellate cells change the direction of migration from radial to tangential, and the somata never enter the EGL. Although it has not yet been determined whether Netrin1-null mice exhibit abnormal migration of stellate/basket cells, present and previous studies suggest that Netrin1, which is present in the EGL, provides a repulsive signal to basket/stellate cells, and alters the direction of basket/stellate cell migration from radial to tangential at the top of the ML. Second, in the cerebellar microexplant cultures, basket/stellate cells sequentially exhibited stereotypical behavior. For example, basket/stellate cells first migrate along the radial fascicles of granule cell axons, then change their orientation perpendicular to the radial fascicles, and subsequently migrate in the perpendicular direction (Hekmat et al., 1989; Magyar-Lehmann et al., 1995), suggesting that contact with the granule cell axons first facilitates basket/stellate cell migration along them, and then induces the changes in the direction of the migration perpendicular to the extension of the axons. This is intriguing because the present study revealed that basket/stellate cells first migrate radially from the IGL to the top of the ML, where the ascending axons of postmigratory granule cells run in parallel. Then, at the top of the ML, basket/stellate cells turn and then migrate tangentially, which is perpendicular to the direction of extension of the parallel fibers (granule cell axons). Taken together, intrinsic programs and cell-cell contact between basket/stellate cells and granule cell axons may be involved in controlling the direction of basket/stellate cell migration in the ML. Future studies are required for elucidating the molecular and cellular mechanisms underlying the control of basket/stellate cell migration.

In this study, we referred to basket cells and stellate cells as basket/stellate cells, and analyzed the migration of both cells as a single cell type. This is because migrating basket cells and stellate cells are morphologically indistinguishable. However, we cannot rule out the possibility that there are some differences in the speed of migration and the transient time in each phase of migration between basket cells and stellate cells.

At present, little is known about the mechanisms underlying the completion of basket/stellate cell migration, but the present study suggests possible mechanisms. For example, at the final stage of migration, basket/stellate cells first withdraw the leading process, then emit multiple dendrite-like processes from the soma, and repeatedly extend and withdraw the processes in multiple directions, while the cells migrate tangentially at their slowest speed. In contrast, during the final stage of migration, cerebellar granule cells, which are excitatory interneurons, exhibit a different order of morphological changes (Komuro and Rakic, 1998a, Kumada and Komuro, 2004; Komuro and Kumada, 2005). For example, at the final stage of migration (within the IGL), the spindle-shaped somata of granule cells round. Then, granules cells gradually slow their movement and become permanently stationary. After the completion of migration, the leading process of granule cells retracts, and then multiple dendrite-like processes emit from the soma. Based on these observations we assume that the differences in the timing of emitting dendrite-like processes from the soma between basket/stellate cells and granule cells play a role in the dispersion of these cells: basket/stellate cells are scattered throughout the ML and granule cells are tightly packed in the IGL. Our hypothesis is that before completing migration, basket/stellate cells try to find their final position, which is away from their older siblings, by examining the vicinity through the extension of dendrite-like processes in multiple directions. On the other hand, granule cells are not required to examine the distance from their older siblings at the final stage of migration. However, the role of extension of multiple dendrite-like processes in the completion of basket/stellate cell migration remains to be determined.

To date, our understanding of mechanisms involved with the migration of basket/stellate cells is very rudimentary. This is because the long lasting uncertainties about the site of origin of these cells did not make them an attractive subject of analysis for neuronal migration. However, there are possible candidates for providing guideposts for migrating basket/stellate cells. First, the Purkinje cell axons, climbing fibers and mossy fibers create a route within the IGL from the bottom to the top (Guijarro et al., 2006). Second, the ascending axons of postmigratory granule cells might serve as a substratum for basket/stellate cell migration from the IGL through the PCL to the ML. Third, Bergmann glial processes may serve as a scaffold for radial migration of basket/stellate cells in the ML. At present, there is no obvious candidate for supporting the tangential migration of basket/stellate cells in the ML. The question of which cells and processes provide guideposts for migrating basket/stellate cells is still open.

Large numbers of molecules and receptors have been discovered as potential regulators or modulators of neuronal cell migration in the developing cerebellum (Komuro and Yacubova, 2003; Yacubova and Komuro, 2003; Jiang et al., 2008; Cameron et al., 2009). For example, extracellular glutamate and the NMDA (N-methyl-D-aspartate) subtype of glutamate receptors are known to control the speed of granule cell migration in the ML (Komuro and Rakic, 1993). Furthermore, brain-derived neurotrophic factor (BDNF) stimulates granule cell migration through the activation of its high affinity receptor (TrkB) (Borghesani et al., 2002). Moreover, neurotrophin-3 accelerates the exit of granule cells from the EGL through the activation of its high affinity receptor (TrkC) (Doughty et al., 1998). Neuregulin receptors (ErbB4 receptors) play a role in granule cell migration along the Bergmann glial fibers in the ML (Rio et al., 1997). Astrotactin and tenascin are also involved in controlling granule cell migration in the ML through regulation of granule cell binding to the Bergmann glial cells (Husmann et al., 1992; Adams et al., 2002). Tissue plasminogen activator affects the speed of

granule cell migration in the ML (Seeds et al., 1999). 9-O-acetyl GD3 (a ganglioside), which is localized at the contact sites between migrating cells and Bergmann glial processes, plays a role in Bergmann glia-associated cell migration in the ML (Santiago et al., 2001). Platelet-activating factor (PAF) and its receptors are required for granule cell migration (Bix and Clark, 1998). Somatostatin differentially controls granule cell migration in a cerebellar cortical layer-specific manner: somatostatin accelerates the tangential migration of granule cells in the EGL, but slows down radial movement in the IGL (Yacubova and Komuro, 2002b). Pituitary adenylate cyclase-activating polypeptide (PACAP) decreases the speed of granule cell migration in the PCL through the activation of its receptor (PAC1) (Cameron et al., 2007, 2009). Finally, stromal cell-derived factor 1α and its receptor CXCR4 control the direction of granule cell migration in the EGL and ML (Ma et al., 1998; Zou et al., 1998). Although the molecules and receptors described above may play a role as potential regulators of basket/stellate cell migration, future studies are required for determining whether these molecules influence basket/stellate cell migration.

Supplementary Material

Refer to Web version on PubMed Central for supplementary material.

Acknowledgments

We thank Y. Komuro for critically reading the manuscript. This work was supported by a Pilot Research Award (PP1450) from the National Multiple Sclerosis Society and a grant (R01 ES015612) from National Institute of Environmental Health Sciences.

References

Adams NC, Tomoda T, Cooper M, Dietz G, Hatten ME. Mice that lack astrotactin have slowed neuronal migration. Development 2002;129:965–972. [PubMed: 11861479]

Altman J. Postnatal development of the cerebellar cortex in the rat. I. The external germinal layer and the transitional molecular layer. J. Comp. Neurol 1972a;145:353–359. [PubMed: 4113154]

Altman J. Postnatal development of the cerebellar cortex in the rat. II. Phases in the maturation of Purkinje cells and of the molecular layer. J. Comp. Neurol 1972b;145:399–463. [PubMed: 5044254]

Anderson SA, Marin O, Horn C, Jennings K, Rubenstein JLR. Distinct cortical migrations from the medial and lateral ganglionic eminences. Development 2001;128:353–363. [PubMed: 11152634]

Ang ESBC, Haydar TF, Gluncic V, Rakic P. Four-dimensional migratory coordinates of GABAergic interneurons in the developing mouse cortex. J. Neurosci 2003;23:5805–5815. [PubMed: 12843285]

Bix GJ, Clark GD. Platelet-activating factor receptor stimulation disrupts neuronal migration *in vitro*. J. Neurosci 1998;18:307–318. [PubMed: 9412509]

Borghesani PR, Peyrin JM, Klein R, Rubin J, Carter AR, Schwartz PM, Luster A, Corfas G, Segal RA. BDNF stimulates migration of cerebellar granule cells. Development 2002;129:1435–1442. [PubMed: 11880352]

Botia B, Basille M, Allais A, Raoult E, Falluel-Morel A, Galas L, Jolivel V, Wurtz O, Komuro H, Fournier A, Vaudry H, Burel D, Gonzalez B, Vaudry D. Neurotrophic effects of PACAP in the cerebellar cortex. Peptides 2007;28:1746–1752. [PubMed: 17544170]

Cameron DB, Galas L, Jiang Y, Raoult E, Vaudry D, Komuro H. Cerebellar cortical-layer-specific control of neuronal migration by pituitary adenylate cyclase-activating polypeptide. Neuroscience 2007;146:697–712. [PubMed: 17383102]

Cameron DB, Raoult E, Galas L, Jiang Y, Lee K, Hu T, Vaudry D, Komuro H. Role of PACAP in controlling granule cell migration. Cerebellum. 2009(in press)

Doughty ML, Lohof A, Campana A, Delhaye-Bouchaud N, Mariani J. Neurotrophin-3 promotes cerebellar granule cell exit from the EGL. Eur. J. Neurosci 1998;10:3007–3011. [PubMed: 9758170]

Fujita S. Quantitative analysis of cell proliferation and differentiation in the cortex of postnatal mouse cerebellum. J. Cell Biol 1967;32:277–287. [PubMed: 10976221]

Fujita S, Shimada M, Nakamura T. H^3-thymidine autoradiographic studies on the cell proliferation and differentiation in the external and the internal granular layers of the mouse cerebellum. J. Comp. Neurol 1966;128:191–208. [PubMed: 5970298]

Ghashghaei HT, Weber J, Penvy L, Schmid R, Schwab MH, Lloyd KC, Eisenstat DD, Lai C, Anton ES. The role of neuregulin-ErbB4 interactions on the proliferation and organization of cells in the subventricular zone. Proc. Natl. Acad. Sci. USA 2006;103:1930–1935. [PubMed: 16446434]

Guerrini R, Filippi T. Neuronal migration disorders, genetics, and epileptogenesis. J. Child Neurol 2005;20:287–299. [PubMed: 15921228]

Guijarro P, Simo S, Pascual M, Abasolo I, Del Rio JA, Soriano E. Netrin1 exerts a chemorepulsive effect on migrating cerebellar interneurons in a Dcc-independent way. Mol. Cell. Neurosci 2006;33:389–400. [PubMed: 17029983]

Hallonet MER, Le Dourain NM. Tracing neuroepithelial cells of the mesencephalic and metencephalic alar plates during cerebellar ontogeny in quail-chick chimeras. Eur. J. Neurosci 1993;5:1145–1155. [PubMed: 8281319]

Hekmat A, Kunemund V, Fischer G, Schachner M. Small inhibitory cerebellar interneurons grow in a perpendicular orientation to granule cell neurites in culture. Neuron 1989;2:1113–1122. [PubMed: 2696503]

Husmann K, Faissner A, Schachner M. Tenascin promotes cerebellar granule cell migration and neurite outgrowth by different domains in the fibronectin type III repeats. J. Cell Biol 1992;116:1475–1486. [PubMed: 1371773]

Jiang Y, Kumada T, Cameron DB, Komuro H. Cerebellar granule cell migration and the effects of alcohol. Dev. Neurosci 2008;30:7–23. [PubMed: 18075250]

Kasai K, Saeki Y. DNA-based methods to prepare helper virus-free herpes amplicon vectors and versatile design of amplicon vector plasmids. Curr. Gene Ther 2006;6:303–314. [PubMed: 16787182]

Kerjan G, Gleeson JG. Genetic mechanisms underlying abnormal neuronal migration in classical lissencephaly. Trends Genet 2007;23:623–630. [PubMed: 17997185]

Komuro H, Kumada T. Ca^{2+} transients control CNS neuronal migration. Cell Calcium 2005;37:387–393. [PubMed: 15820385]

Komuro H, Rakic P. Selective role of N-type calcium channels in neuronal migration. Science 1992;257:806–809. [PubMed: 1323145]

Komuro H, Rakic P. Modulation of neuronal migration by NMDA receptors. Science 1993;260:95–97. [PubMed: 8096653]

Komuro H, Rakic P. Dynamics of granule cell migration: a confocal microscopic study in acute cerebellar slice preparations. J. Neurosci 1995;15:1110–1120. [PubMed: 7869087]

Komuro H, Rakic P. Intracellular Ca^{2+} fluctuations modulate the rate of neuronal migration. Neuron 1996;17:275–285. [PubMed: 8780651]

Komuro H, Rakic P. Distinct modes of neuronal migration in different domains of developing cerebellar cortex. J. Neurosci 1998a;18:1478–1490. [PubMed: 9454856]

Komuro H, Rakic P. Orchestration of neuronal migration by activity of ion channels, neurotransmitter receptors, and intracellular Ca^{2+} fluctuations. J. Neurobiol 1998b;37:110–130. [PubMed: 9777736]

Komuro, H.; Rakic, P. In vitro analysis of signal mechanisms involved in neuronal migration. In: Haynes, LW., editor. The neuron in tissue culture. New York: John Wiley & Sons; 1999. p. 57-69.

Komuro H, Yacubova E. Recent advances in cerebellar granule cell migration. Cell. Mol. Life Sci 2003;60:1084–1098. [PubMed: 12861377]

Komuro H, Yacubova E, Yacubova E, Rakic P. Mode and tempo of tangential cell migration in the cerebellar external granular layer. J. Neurosci 2001;21:527–540. [PubMed: 11160432]

Kriegstein AR, Noctor SC. Pattern of neuronal migration in the embryonic cortex. Trends Neurosci 2004;27:392–399. [PubMed: 15219738]

Kumada T, Komuro H. Completion of neuronal migration regulated by loss of Ca^{2+} transients. Proc. Natl. Acad. Sci. USA 2004;101:8479–8484. [PubMed: 15150416]

Kumada T, Lakshmana MK, Komuro H. Reversal of Neuronal migration in a mouse model of fetal alcohol syndrome by controlling second-messenger signalings. J. Neurosci 2006;26:742–756. [PubMed: 16421294]

Kumada T, Jiang Y, Cameron DB, Komuro H. How does alcohol impair neuronal migration? J. Neurosci. Res 2007;85:465–470. [PubMed: 17139684]

Kumada T, Jiang Y, Kawanami A, Cameron DB, Komuro H. Autonomous turning of cerebellar granule cells *in vitro* by intrinsic programs. Dev. Biol 2009;326:237–259. [PubMed: 19063877]

Leto K, Carletti B, Williams IM, Magrassi L, Rossi F. Different types of cerebellar GABAergic interneurons originate from a common pool of multipotent progenitor cells. J. Neurol 2006;26:11682–11694.

Ma Q, Jones D, Borghesani PR, Segal RA, Nagasawa T, Kishimoto T, Bronson RT, Springer TA. Impaired B-lymphopoiesis, myelopoiesis, and derailed cerebellar neuron migration in CXCR4-and SDF-1-deficient mice. Proc. Natl. Acad. Sci. USA 1998;95:9448–9453. [PubMed: 9689100]

Magyar-Lehmann S, Suter CS, Stahel W, Schachner M. Behaviour of small inhibitory interneurons in early postnatal mouse cerebellar microexplant cultures: a video time-lapse analysis. Eur. J. Neurosci 1995;7:1449–1459. [PubMed: 7551171]

Maricich SM, Herrup K. Pax-2 expression defines a subset of GABAergic interneurons and their precursors in the developing murine cerebellum. J. Neurobiol 1999;41:281–294. [PubMed: 10512984]

Marin O, Rubenstein JLR. A long, remarkable journey: tangential migration in the telencephalon. Nat. Rev. Neurosci 2001;2:780–790. [PubMed: 11715055]

Marin O, Rubenstein JLR. Cell migration in the forebrain. Ann. Rev. Neurosci 2003;26:441–483. [PubMed: 12626695]

Miale I, Sidman RL. An autoradiographic analysis of histogenesis in the mouse cerebellum. Exp. Neurol 1961;4:277–296. [PubMed: 14473282]

Milosevic A, Goldman JE. Progenitors in the postnatal cerebellar white matter are antigenically heterogeneous. J. Comp. Neurol 2002;452:192–203. [PubMed: 12271492]

Milosevic A, Goldman JE. Potential of progenitors from postnatal cerebellar neuroepithelium and white matter: lineage specified vs. multipotent fate. Mol. Cell. Neurosci 2004;26:342–353.

Nadarajah B, Parnavelas JG. Modes of neuronal migration in the developing cerebral cortex. Nat. Rev. Neurosci 2002;4:143–150.

Napieralski JA, Eisenman LM. Developmental analysis of the external granular layer in the meander tail mutant mouse: do cerebellar microneurons have independent progenitors? Dev. Dynamics 1993;197:244–254.

Otero RA, Sotelo C, Alvarado-Mallart R-M. Chick/quail chimeras with partial cerebellar grafts: an analysis of the origin and migration of cerebellar cells. J. Comp. Neurol 1993;333:597–615. [PubMed: 7690372]

Pang T, Atefy R, Sheen V. Malformations of cortical development. Neurologist 2008;14:181–191. [PubMed: 18469675]

Rakic P. Neuron-glia relationship during granule cell migration in developing cerebellar cortex. A golgi and electron microscopic study in Macacus rhesus. J. Comp. Neurol 1971;141:283–312. [PubMed: 4101340]

Rakic P. Kinetics of proliferation and latency between final cell division and onset of differentiation of cerebellar stellate and basket neurons. J. Comp. Neurol 1973;147:523–546. [PubMed: 4122708]

Rakic P. Principles of neuronal cell migration. Experientia 1990;46:882–891. [PubMed: 2209797]

Rakic P. Molecular and cellular mechanisms of neuronal migration: relevance to cortical epilepsies. Adv. Neurol 2000;84:1–14. [PubMed: 11091853]

Rakic P, Komuro H. The role of receptor/channel activity in neuronal cell migration. J. Neurobiol 1995;26:299–315. [PubMed: 7775964]

Rakic P, Cameron RS, Komuro H. Recognition, adhesion, transmembrane signaling and cell motility in guided neuronal migration. Curr. Opin. Neurobiol 1994;4:63–69. [PubMed: 8173327]

Rio C, Rieff HI, Qi P, Khurana TS, Corfas G. Neuregulin and erbB receptors play a critical role in neuronal migration. Neuron 1997;19:39–50. [PubMed: 9247262]

Saeki Y, Breakefield XO, Chiocca EA. Improved HSV-1 amplicon packaging system using ICP27-deleted, oversized HSV-1 BAC DNA. Methods Mol. Med 2003;76:51–60. [PubMed: 12526158]

Saeki Y, Fraefel C, Ichikawa T, Breakefield XO, Chiocca EA. Improved helper virus-free packaging system for HSV amplicon vectors using an ICP27-deleted, oversized HSV-1 DNA in a bacterial artificial chromosome. Mol. Ther 2001;3:591–601. [PubMed: 11319922]

Santiago MF, Berredo-Pinho M, Costa MR, Gandra M, Cavalcante LA, Mendez-Otero R. Expression and function of ganglioside 9-O-acetyl GD3 in postmitotic granule cell development. Mol. Cell. Neurosci 2001;17:488–499. [PubMed: 11273644]

Seeds NW, Basham ME, Haffke SP. Neuronal migration is retarded in mice lacking the tissue plasminogen activator gene. Proc. Natl. Acad. Sci. USA 1999;96:14118–14123. [PubMed: 10570208]

Smith IL, Hardwicke MA, Sandri-Goldin RM. Evidence that the herpes simplex virus immediate early protein ICP27 acts post-transcriptionally during infection to regulate gene expression. Virology 1992;186:74–86. [PubMed: 1309283]

Tanaka D, Maekawa K, Yanagawa Y, Obata K, Murakami F. Multidirectional and multizonal tangential migration of GABAergic interneurons in the developing cerebral cortex. Development 2006;133:2167–2176. [PubMed: 16672340]

Tanaka DH, Yanagida M, Zhu Y, Mikami S, Nagasawa T, Miyazaki J, Yanagawa Y, Obata K, Murakami F. Random walk behavior of migrating cortical interneurons in the marginal zone: time-lapse analysis in flat-mount cortex. J. Neurol 2009;29:1300–1311.

Tashiro Y, Yanagawa Y, Obata K, Murakami F. Development and migration of GABAergic neurons in the mouse myelencephalon. J. Comp. Neurol 2007;503:260–269. [PubMed: 17492625]

Ten Donkelaar HJ, Lammens M, Wesseling P, Thijessen HO, Renier WO. Development and developmental disorders of the human cerebellum. J. Neurol 2003;250:1025–1036. [PubMed: 14504962]

Weisheit G, Gliem M, Endl E, Pfeffer PL, Busslinger M, Schilling K. Postnatal development of the murine cerebellar cortex: formation and early dispersal of basket, stellate and Golgi neurons. Eur. J. Neurosci 2006;24:466–478. [PubMed: 16903854]

Yacubova E, Komuro H. Intrinsic program for migration of cerebellar granule cells *in vitro*. J. Neurosci 2002a;22:5966–5981. [PubMed: 12122059]

Yacubova E, Komuro H. Stage-specific control of neuronal migration by somatostatin. Nature 2002b; 415:77–81. [PubMed: 11780120]

Yacubova E, Komuro H. Cellular and molecular mechanisms of cerebellar granule cell migration. Cell Biochem. Biophys 2003;37:213–234. [PubMed: 12625628]

Yamanaka H, Yanagawa Y, Obata K. Development of stellate and basket cells and their apoptosis in mouse cerebellar cortex. Neurosci. Res 2004;50:13–22. [PubMed: 15288494]

Yip J, Soghomonian J-J, Blatt GJ. Increased GAD67 mRNA expression in cerebellar interneurons in autism: implications for Purkinje cell dysfunction. J. Neurosci. Res 2008;86:525–530. [PubMed: 17918742]

Zhang L, Goldman JE. Generation of cerebellar interneurons from dividing progenitors in white matter. Neuron 1996a;16:47–54. [PubMed: 8562089]

Zhang L, Goldman JE. Developmental fates and migratory pathways of dividing progenitors in the postnatal rat cerebellum. J. Comp. Neurol 1996b;370:536–550. [PubMed: 8807453]

Zou YR, Kottmann AH, Kuroda M, Taniuchi I, Littman DR. Function of the chemokine receptor CXCR4 in haematopoiesis and in cerebellar development. Nature 1998;393:595–599. [PubMed: 9634238]

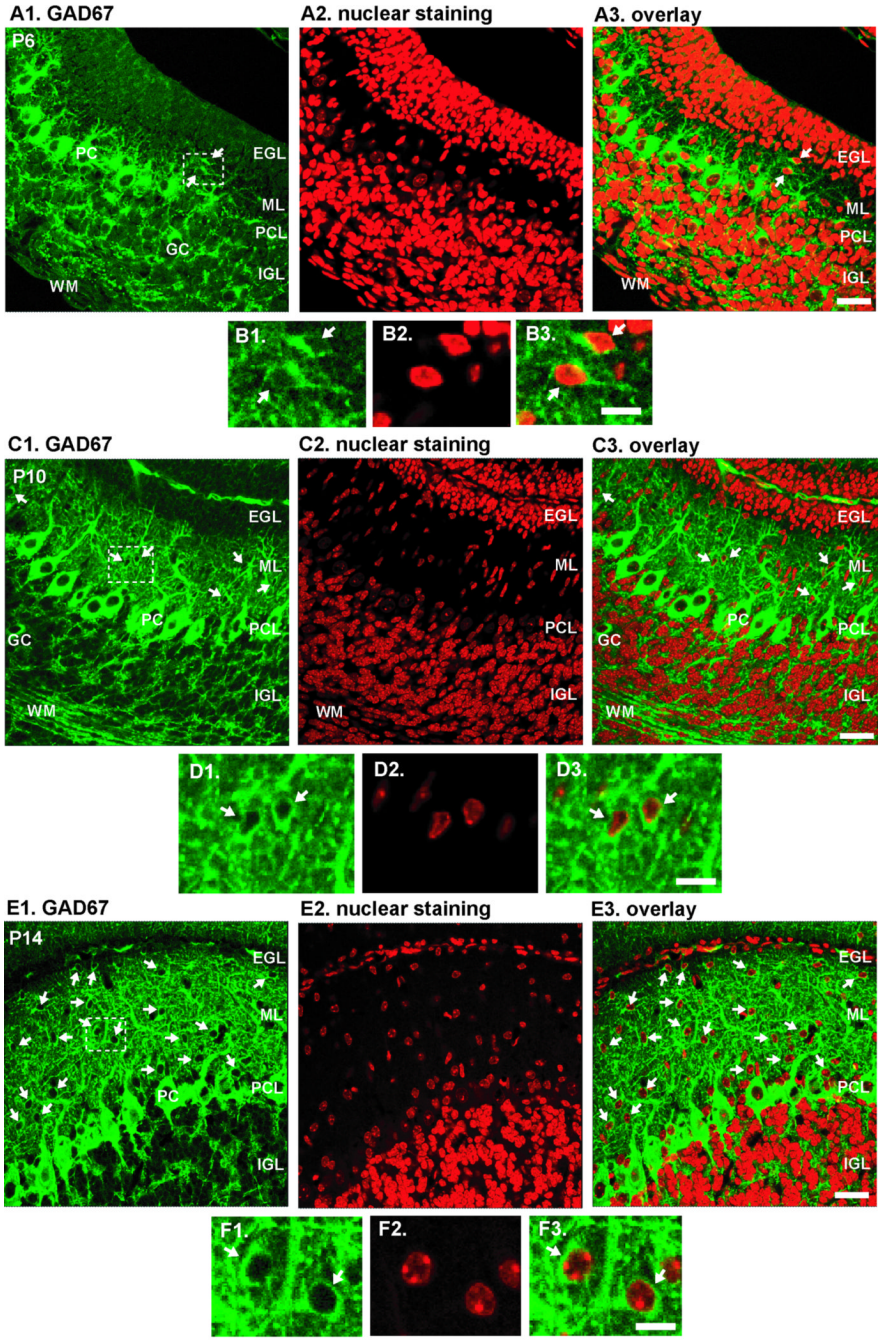

Fig. 1.

Expression of GAD67 in the early postnatal mouse cerebella. (A1, C1, E1) Expression of GAD67 in the sagittal sections of P6 (A1), P10 (C1) and P14 (E1) mouse cerebella, respectively. (A2, C2, E2) Nuclear staining of the sections presented in A1, C1, E1, respectively. (A3, C3, E3) Superimposed image of A1 and A2 (in A3), C1 and C2 (in C3), E1 and E3 (in E3), respectively. (B1–B3) Enlarged images of the boxed area presented in A1. (D1–D3) Enlarged images of the boxed area presented in C1. (F1–F3) Enlarged images of the boxed area presented in E1. Scale Bars (in μm): 60 (A3, C3, E3); 12 (B3, D3, F3). White arrows represent GAD-expressing stellate/basket cells in the ML. Abbreviations: EGL, external

granular layer; Ml, molecular layer; PCL, Purkinje cell layer; IGL, internal granular layer; WM, white matter; PC, Purkinje cells, GC, Golgi cells

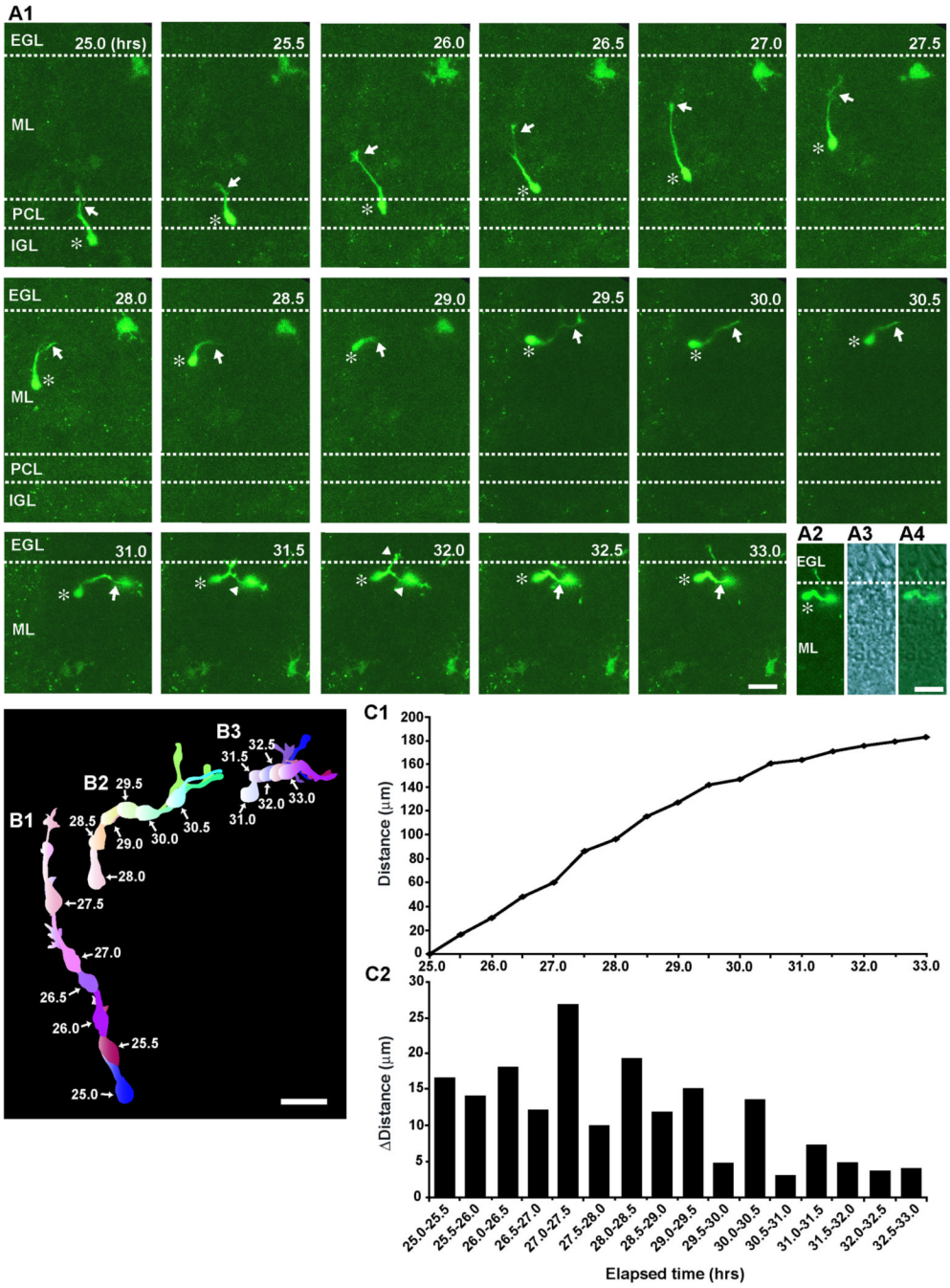

Fig. 2.

Radial migration of a stellate/basket cell from the top of the IGL through the PCL to the top of the ML, and subsequent change in the direction of migration from radial to tangential at the top of the ML. (A1) Time-lapse series of images showing the migration of a stellate/basket cell from the IGL through the PCL to the top of the ML of P9 mouse cerebellum. Elapsed time after *in vitro* (in hours) is indicated on the top-right of each photograph. Asterisks and arrows mark the soma and the leading process, respectively. Arrowheads represent the branch of the leading process. Scale bar; 24 μm. (A2-A4) Superimposed image (A4) of a fluorescent image (A2) and a transmitted image (A3) obtained at 32 hours after *in vitro* in A1. An asterisk marks the soma. A scale bar; 24 μm. (B1–B3) Pseudocolor images represent images of a stellate/

basket cell taken every half hour shown in A1. Six images of the cell are superimposed in both B1 and B2, and five images are superimposed in B3. The numbers represent elapsed time after *in vitro* (in hours). Scale bar; 20 μm. (C1 and C2) The total distance traversed by the cell (C1) shown in A1 and the direction and distance traveled by the cell during each half hour of the testing period (C2) were plotted as a function of elapsed time after *in vitro*

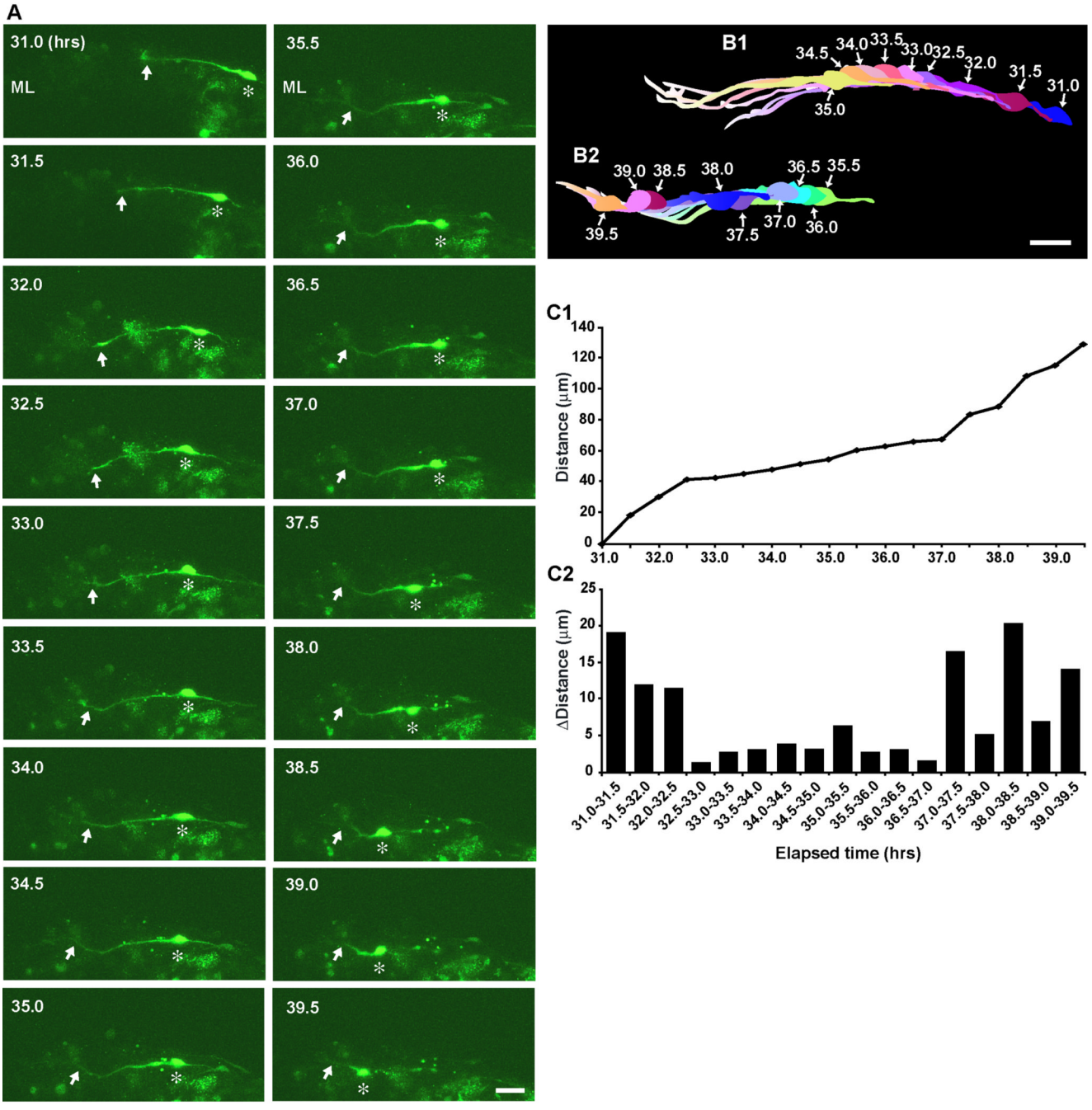

Fig. 3.

Tangential migration of a stellate/basket cell at the top of the ML. (A) Time-lapse series of images showing the tangential migration of a stellate/basket cell at the top of the ML of P9 mouse cerebellum. Elapsed time after *in vitro* (in hours) is indicated on the top-left of each photograph. Asterisks and arrows mark the soma and the leading process, respectively. Scale bar; 25 μm. (B1 and B2) Pseudocolor images represent images of the stellate/basket cell taken every half hour shown in A. Nine images of the cell are superimposed in both B1 and B2. The numbers represent elapsed time after *in vitro* (in hours). Scale bar; 17 μm. (C1 and C2) The total distance traversed by the cell (C1) shown in A and the direction and distance traveled by

the cell during each half hour of the testing period (C2) were plotted as a function of elapsed time after *in vitro*

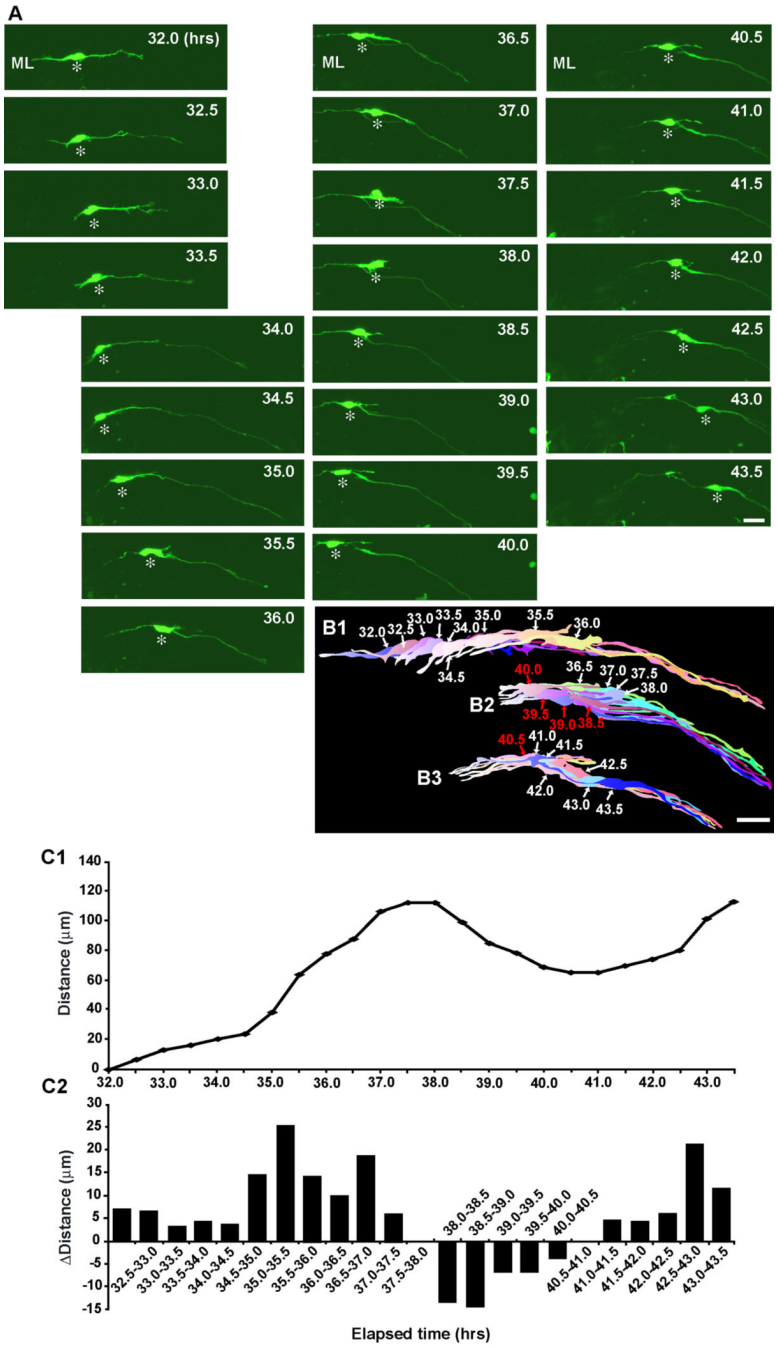

Fig. 4.

Reversal of the direction of tangential migration of a stellate/basket cell at the top of the ML. (A) Time-lapse series of images showing the reversal of tangential migration of a stellate/basket cell at the top of the ML of P9 mouse cerebellum. Elapsed time after *in vitro* (in hours) is indicated on the top-right of each photograph. Asterisks mark the soma. Scale bar; 21 μm. (B1-B3) Pseudocolor images represent images of the stellate/basket cell taken every half hour shown in A. Nine images, eight images, and seven images of the cell are superimposed in B1, B2, and B3, respectively. The numbers represent elapsed time after *in vitro* (in hours). Scale bar; 22 μm. (C1 and C2) The total distance traversed by the cell (C1) shown in A and the direction and distance traveled by the cell during each half hour of the testing period (C2) were

plotted as a function of elapsed time after *in vitro*. In C2, positive values represent tangential cell movement towards the rostral direction, while negative values represent tangential cell movement towards the caudal direction.

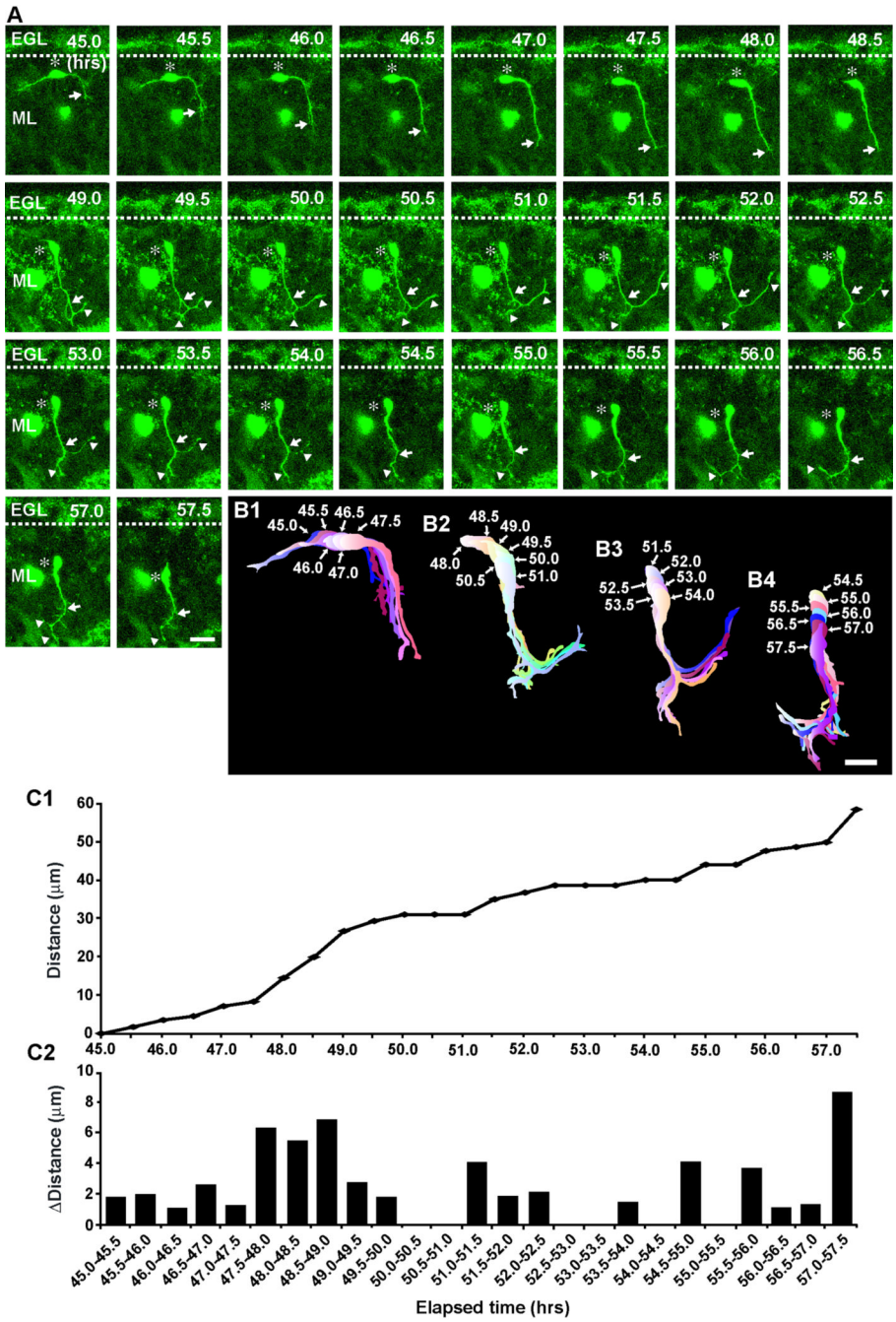

Fig. 5.

Alterations of the direction of stellate/basket cell migration from tangential to radial at the top of the ML. (A) Time-lapse series of images showing the change in the direction of stellate/basket cell migration in the ML of P10 mouse cerebellum. Elapsed time after *in vitro* (in hours) is indicated on the top right of each photograph. Asterisks mark the soma. Arrows and arrowheads represent the leading process of a stellate/basket cell and the branches, respectively. Scale bar; 20 μm. (B1–B4) Pseudocolor images represent images of the stellate/basket cell taken every half hour shown in A. Six images, seven images, six images, and seven images of the cell are superimposed in B1, B2, B3, and B4, respectively. The numbers represent elapsed time after *in vitro* (in hours). Scale bar; 22 μm. (C1 and C2) The total distance traversed by

the cell (C1) shown in A and the direction and distance traveled by the cell during each half hour of the testing period (C2) were plotted as a function of elapsed time after *in vitro*

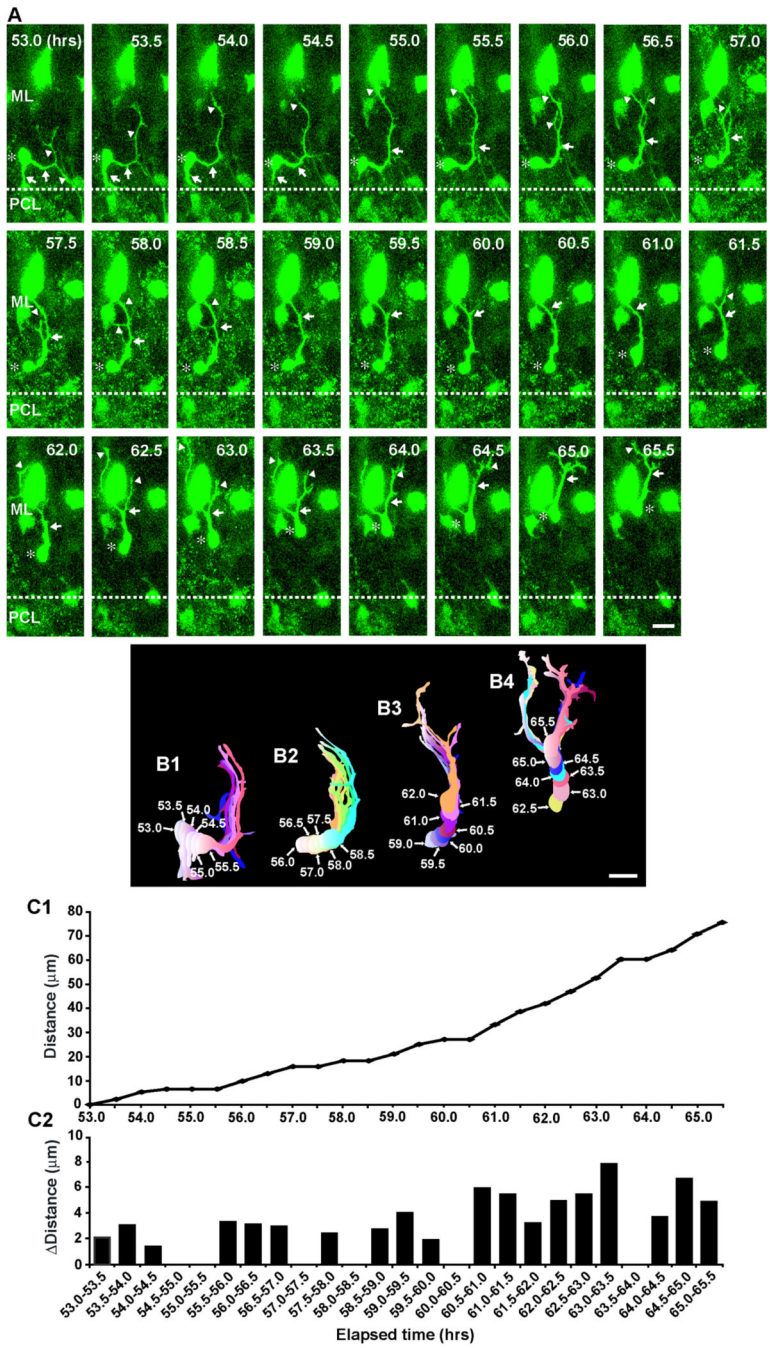

Fig. 6.

Turning of a stellate/basket cell at the bottom of the ML. (A) Time-lapse series of images showing the change of the direction of stellate/basket cell migration at the bottom of the ML of P10 mouse cerebellum. Elapsed time after *in vitro* (in hours) is indicated on the top right of each photograph. Asterisks mark the soma. Arrows and arrowheads represent the leading process of a stellate/basket cell and the branches, respectively. Scale bar; 15 μm. (B1-B4) Pseudocolor images represent images of the stellate/basket cell taken every half hour shown in A. Six images of the cell are superimposed in both B1 and B2, and seven images of the cell are superimposed in both B3 and B4. The numbers represent elapsed time after *in vitro* (in hours). Scale bar; 18 μm. (C1 and C2) The total distance traversed by the cell (C1) shown in

A and the direction and distance traveled by the cell during each half hour of the testing period (C2) were plotted as a function of elapsed time after *in vitro*

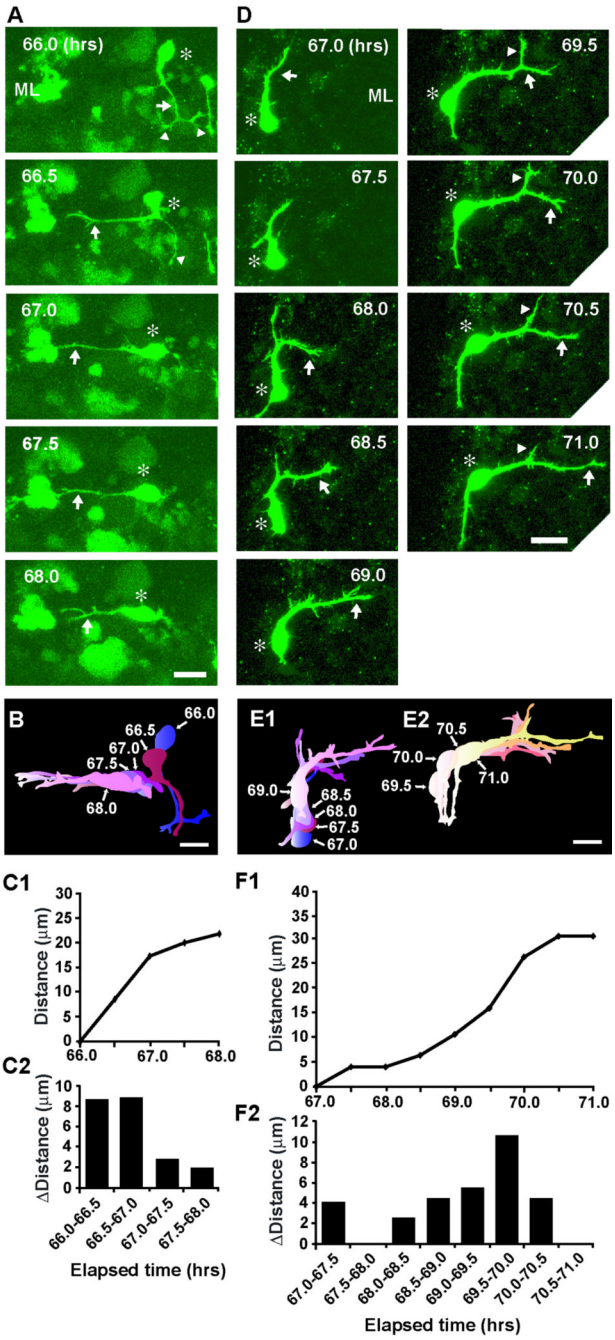

Fig. 7.

Final turning of stellate/basket cells at the middle of the ML. (A and D) Time-lapse series of images showing the direction of stellate/basket cell migration from radial to tangential at the middle of the ML of P10 mouse cerebellum. Elapsed time after *in vitro* (in hours) is indicated on the top right of each photograph. Asterisks mark the soma. Arrows and arrowheads represent the leading processes of stellate/basket cells and their branches, respectively. Scale bars; 13 μm in A, and 15 μm in D. (B) Pseudocolor images represent images of the stellate/basket cell taken every half hour shown in A. Five images of the cell are superimposed in B. (E1 and E2) Pseudocolor images represent images of the stellate/basket cell taken every half hour shown in D. Five images of the cell are superimposed in E1, and four images of the cell are

superimposed in E2. In B, E1 and E2, the numbers represent elapsed time after *in vitro* (in hours). Scale bars; 15 μm in B, and 14 μm in E1 and E2. (C1 and F1) The total distance traversed by the cell (C1) shown in A and the cell (F1) shown in D were plotted as a function of elapsed time after *in vitro*. (C2 and F2) The direction and distance traveled by the cell (C2) shown in A and the cell (F2) shown in D during each half hour of the testing period were plotted as a function of elapsed time after *in vitro*.

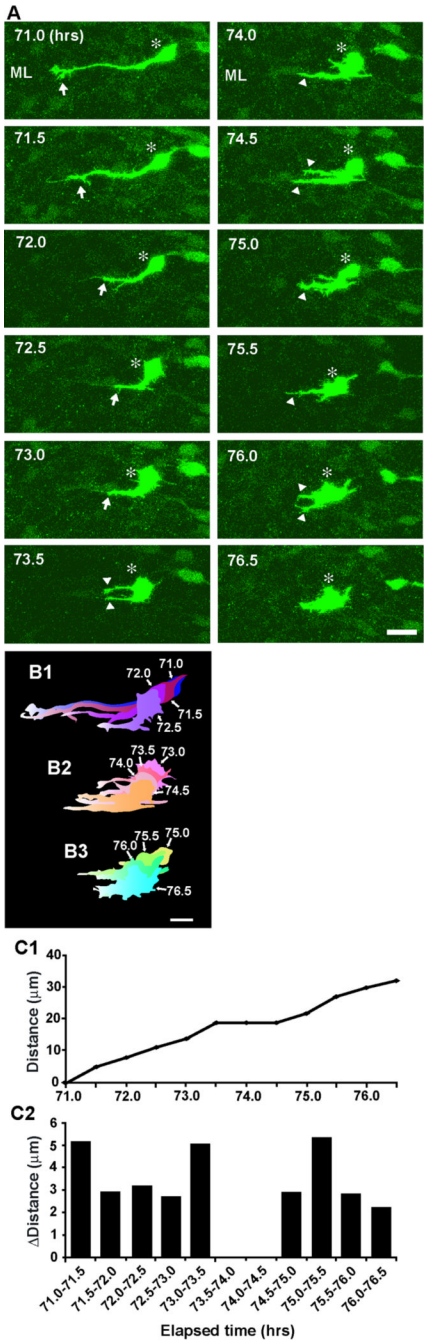

Fig. 8.

Initial sign of the completion of stellate/basket cell migration in the middle of the ML. (A) Time-lapse series of images showing the withdrawal of the leading process of stellate/basket cells at the middle of the ML of P10 mouse cerebellum. Elapsed time after *in vitro* (in hours) is indicated on the top left of each photograph. Asterisks mark the soma. Arrows and arrowheads represent the leading process of a stellate/basket cell and the neuronal processes, respectively. Scale bar; 12 μm. (B1-B3) Pseudocolor images represent images of the stellate/basket cell taken every half hour shown in A. Four images of the cell are superimposed in B1, B2 and B3, respectively. The numbers represent elapsed time after *in vitro* (in hours). Scale bar; 10 μm. (C1 and C2) The total distance traversed by the cell (C1) shown in A and the

direction and distance traveled by the cell during each half hour of the testing period (C2) were plotted as a function of elapsed time after *in vitro*.

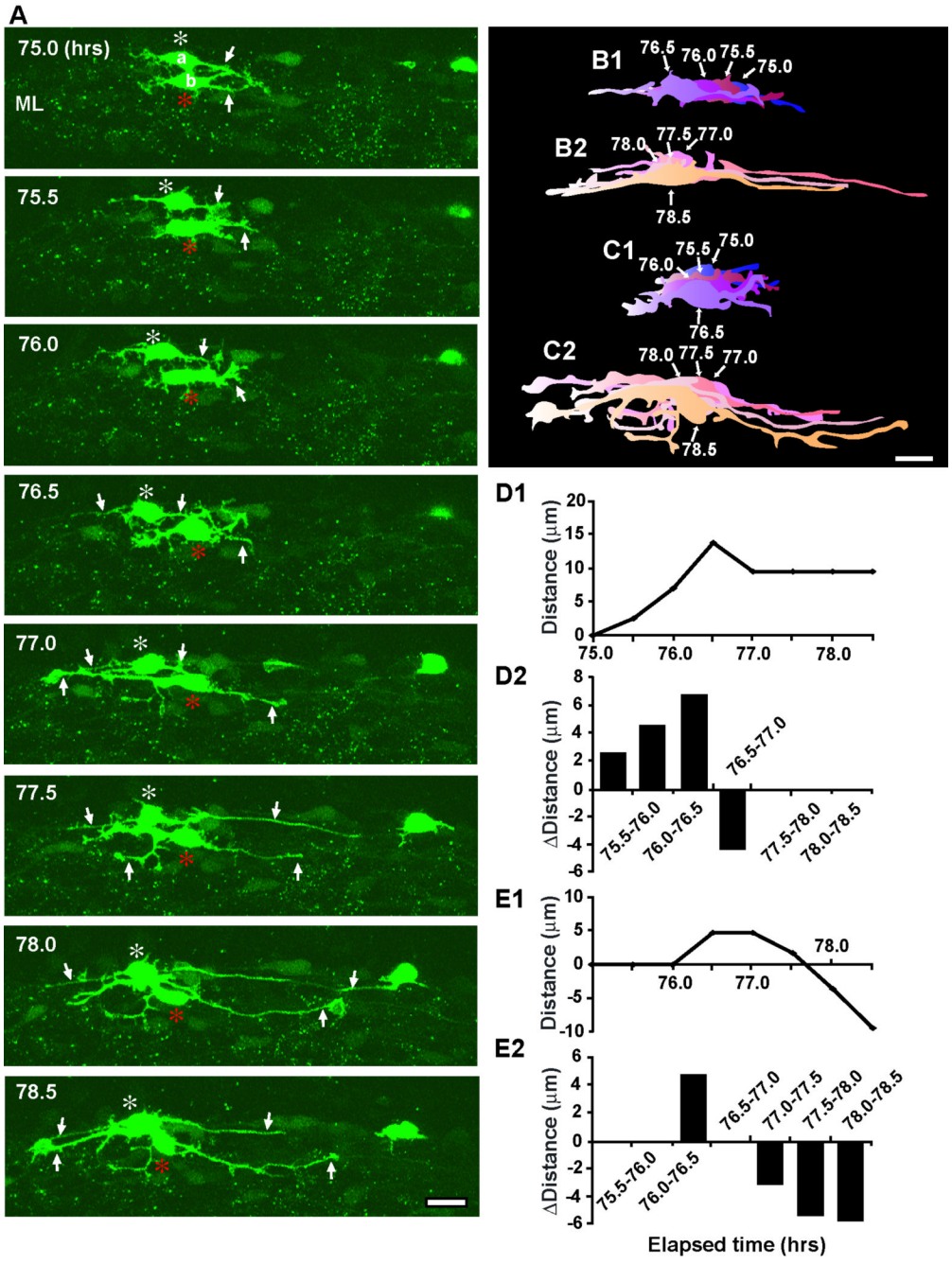

Fig. 9.

Extension of dendrite-like processes while migrating tangentially in the middle of the ML. (A) Time-lapse series of images showing the extension of dendrite-like processes from the somata of stellate/basket cells in the middle of the ML of P9 mouse cerebellum. Elapsed time after *in vitro* (in hours) is indicated on the top left of each photograph. White and red asterisks mark the somata of two stellate/basket cells (a and b), respectively. Arrows represent the dendrite-like processes. Scale bar; 13 μm. (B1 and B2) Four images of the cell (marked by a in A) are superimposed in both B1 and B2, respectively. (C1 and C2) Four images of the cell (marked by b in A) are superimposed in both C1 and C2, respectively. In B1, B2 and C1, C2, the numbers represent the elapsed time after *in vitro* (hours). Scale bar; 10 μm. (D1 and D2) The total

distance traversed by the cell (D1) (marked by a in A) and the direction and distance traveled by the cell during each half hour of the testing period (D2) were plotted as a function of elapsed time after *in vitro*. (E1 and E2) The total distance traversed by the cell (E1) (marked by b in A) and the direction and distance traveled by the cell during each half hour of the testing period (E2) were plotted as a function of elapsed time after *in vitro*. In D2 and E2, positive values represent forward cell movement, while negative values represent backward cell movement.

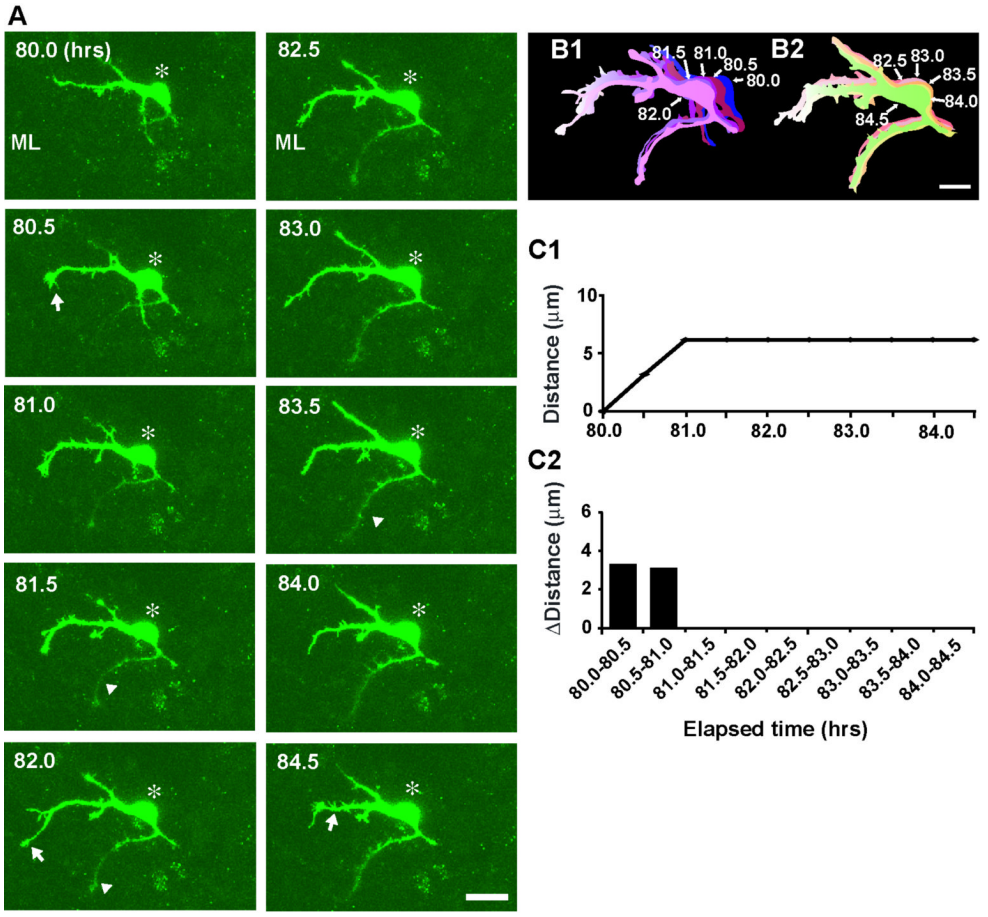

Fig. 10.

Completion of stellate/basket cell migration at the middle of the ML. (A) Time-lapse series of images showing the completion of stellate/basket cell migration at the middle of the ML of P9 mouse cerebellum. Elapsed time after *in vitro* (in hours) is indicated on the top left of each photograph. Asterisks mark the soma. Arrows and arrowheads represent the dendrite-like processes. Scale bar; 11 μm. (B1 and B2) Pseudocolor images represent images of the stellate/basket cell taken every half hour shown in *A*. Five images of the cell in A are superimposed in both B1 and B2, respectively. The numbers represent elapsed time after *in vitro* (in hours). Scale bar; 10 μm. (C1 and C2) The total distance traversed by the cell (C1) in A and the direction and distance traveled by the cell during each half hour of the testing period (C2) were plotted as a function of elapsed time after *in vitro*.

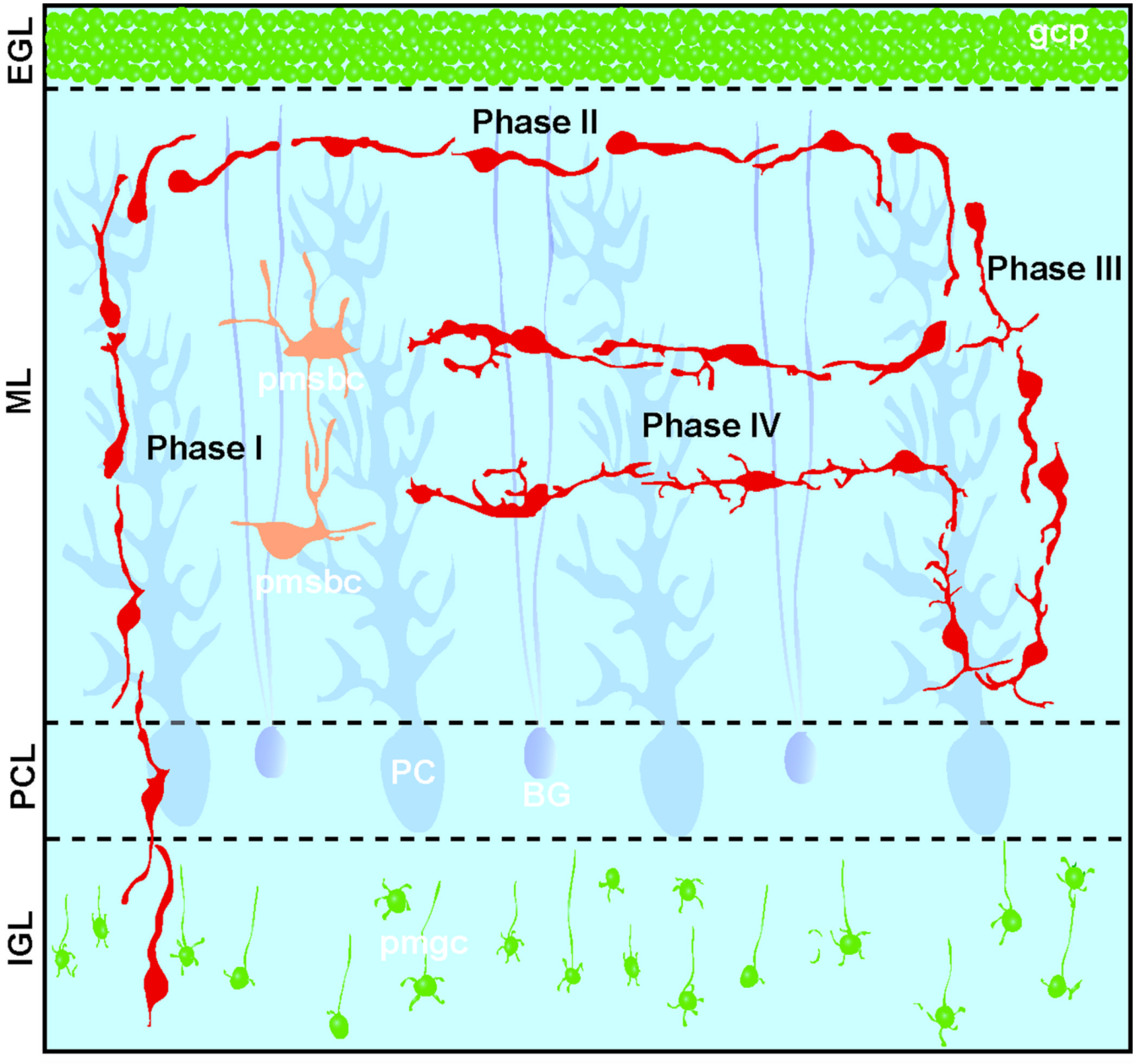

Fig. 11.

Four distinct phases of basket/stellate cell migration in the ML of the developing cerebellum. Abbreviations: gcp, granule cell precursors; pmsbc, postmigratory stellate/basket cells; pmgc, postmigratory granule cells; BG, Bergmann glial cells; PC, Purkinje cells.